

Thermokinetic Transport Control and Structural Microscopic
Realities in Coal and Polymer Pyrolysis and Devolatilization:
Their Dominant Role in Dust Explosions

By M. Hertzberg, I. A. Zlochower, R. S. Conti, and K. L. Cashdollar

U. S. Bureau of Mines
Pittsburgh Research Center
P.O. Box 18070
Cochrans Mill Road
Pittsburgh, PA 15236

ABSTRACT

The reaction mechanism for coal pyrolysis and devolatilization involves the inward progression from the exposed surface of a decomposition wave, whose speed of propagation determines the pyrolysis rate. The speed is controlled by the heat flux driving the wave and by thermodynamic transport constraints within the particle. Microscopic data are presented that reveal the structure of that wave front for unidirectional laser exposure of both macroscopic coal samples and microscopic dust particles. At burner-level heat fluxes of 100 to 125 W/cm², the wave front thickness is less than 50 μm.

New data are also presented for polymethylmethacrylate (PMMA) at flux levels of 12-115 W/cm² that give a pyrolysis and devolatilization "rate coefficient" of,

$$k_t = \left\{ \int_{T_0}^{T_g} C(T) dT + \Delta H_V \right\}^{-1},$$

whose value is predictable from thermodynamic transport constraints alone. Except for the complication of the coal's char-layer residue and its increasing thickness, which insulates the wave front from the heat source flux that drives it, both coal and PMMA behave similarly. For PMMA, the decomposition temperature, T_g , is 350-400° C; for coal it is 450-600° C.

There is no substantive evidence to support the traditional viewpoint that the reaction processes occur isothermally under chemical rate control and that they are describable by unimolecular, Arrhenius functions of the source temperature.

The volatility yield of a dust and its rate of devolatilization play dominant roles in the overall mechanism of flame propagation in dust-air mixtures. Data for the particle size dependences of the lean limits of flammability for coals and polymers reveal those roles. The above measured rate coefficient for PMMA gives a reasonable prediction of the coarse size at which the particle devolatilization process becomes rate limiting in a PMMA dust explosion.

INTRODUCTION

Two theories or models have been used to describe the process of coal particle pyrolysis and devolatilization. The first is the traditional viewpoint, which considers the reaction process to be under chemical rate control (1, 2, 3); the second is a newer viewpoint that considers the reaction process to be under heat transport control (4, 5, 6, 7). In the traditional model the reaction or reactions are viewed as occurring isothermally throughout the particle and are described by classical, unimolecular, Arrhenius functions of the particle temperature, T . The reaction rate is given by

$$\frac{dV(t)}{dt} = k_0 [e^{-E_a/RT}] [V(\infty) - V(t)], \quad (1)$$

where $V(t)$ is the volatile yield (in pct) after an exposure time, t ; $V(\infty)$ is the maximum volatile yield as $t \rightarrow \infty$; k_0 is the preexponential factor; E_a is the activation energy; R is the universal gas constant; and T is the temperature of the pyrolyzing particle. Considerable effort has gone into the development of complex, parallel or sequential reaction schemes to predict the overall rate of pyrolysis and the yields of volatile products. Surprisingly, however, little effort has been devoted to a realistic analysis of the heat transport processes by which particle temperatures, initially at T_0 , are elevated to the reaction temperature T after

their exposure to some high temperature source at T_h . Early researchers generally assumed that the exposed coal particles rapidly reached the high temperatures of the furnace walls, or the hot gases, or the electrically-heated screens to which they were exposed. The temperature used in Equation 1 was generally the source temperature, T_h . A major exception was Zielinski (7), whose independent analysis of the data of many investigators led to the conclusion that the rate of the heat transfer from the high-temperature source to the coal particles exerted the dominant influence on the rate of volatiles evolution. He noted that coal particle temperature measurements were "very rare indeed," and cautioned researchers against assigning "the temperature of the heat carrier or the container walls" to the temperature of "the coal particles themselves." Zielinski's analysis was generally ignored until the more recent studies of Fréihaut and Vastola (8), and the reanalysis of particle pyrolysis data by Solomon and coworkers (9, 10). Using direct optical measurements of particle temperatures, Solomon et al. (10) showed clearly that, during pyrolysis, T was generally much lower than T_h . For example, in an entrained flow reaction at a source temperature of $T_h = 1300^\circ\text{C}$, coal particles of 45-75 μm diameter were completely devolatilized by the time they had reached temperatures of only 700-800 $^\circ\text{C}$. Their analysis is nevertheless limited to the problem of heat transfer to the particle; the particle itself is still treated as reacting isothermally, and uniformly throughout its extent. Internal variations in temperature and reaction rate are ignored. Since, however, the particle is not isothermal, one must go even further in the reanalysis. For coal, especially, there is inevitably a hotter, opaque char layer at the surface of the particle that surrounds and conceals the lower temperature region of active pyrolysis further within the particle.

Accordingly, not only must one consider heat transport limitations to the particle from the external heat source, but also heat transport limitations within or through the particle; that is, from its surface to its interior. Attempts to address that limitation lead to the newer viewpoint or model. The situation in its simplest form is depicted in Figure 1, and the newer theory simply applies the First Law of Thermodynamics to the system. A planar coal surface is depicted, pyrolyzing and devolatilizing at a steady-state rate, \dot{x}_0 , in an incident radiative source flux of intensity, I . The system depicted is coal, which is complicated by a char residue above the pyrolysis reaction zone. Initially, it will be simpler to assume that the reactant is one that devolatilizes completely so that the incident flux is absorbed directly at the devolatilizing surface. Polymethylmethacrylate (PMMA) is an example of such a substance. A fraction of the incident flux, r_1 , is reflected, and another portion, I_L , is lost to the colder surroundings by conduction, convection, and reradiation. For the steady-state propagation of the pyrolysis wave, at the liner rate, \dot{x}_0 , the First Law requires that the net absorbed flux, $I_{\text{abs}} = I(1-r) - I_L$, first supply the power necessary to bring each element of the solid reactant with its heat capacity $C(T)$ to the reaction zone or decomposition temperature, T_S , from its initial temperature, T_0 ; and second, supply the heat of devolatilization. Thus,

$$I_{\text{abs}} = I(1 - r) - I_L = \dot{x}_0 \rho \left[\int_{T_0}^{T_S} C(T) dT + \Delta H_V \right]. \quad (2)$$

Solving for the mass devolatilization rate per unit area gives

$$\dot{m} = \dot{x}_0 \rho = k_t I_{\text{abs}} = \left[\int_{T_0}^{T_S} C(T) dT + \Delta H_V \right]^{-1} I_{\text{abs}}, \quad (3)$$

where the rate coefficient, k_t , is given by the reciprocal of the net enthalpy change for the overall heating and devolatilization process.

This newer viewpoint should be contrasted with the traditional one. In this flux-driven, heat-transport-limited model (Equations 2 and 3), once the input flux level exceeds some critical value for the onset of reaction, which is the loss flux, the predicted rate is not particularly sensitive to the reaction zone temperature of the pyrolyzing surface. That temperature, T_S , is only the upper bound of a heat capacity integral. The rate coefficient, k_t , is much more sensitive to the heat of devolatilization or vaporization, ΔH_V . By contrast, in the traditional viewpoint (Equation 1), the reaction temperature T is the only variable determining the rate. In the flux-driven model, the system is nonisothermal and the exact temperature of

the reacting surface becomes virtually irrelevant once it reaches some threshold value. The traditional viewpoint, by contrast, focuses on that one intensive thermodynamic variable, T, and it does so only in one region of the system, the reaction zone. The newer viewpoint emphasizes extensive thermodynamic variables: The absorbing flux, I_{abs} , and the overall enthalpy change for the pyrolysis and devolatilization process, quite independent of the temperature of any one region of the nonisothermal system. In the newer model, the driving force for the reaction is the net energy flux density being absorbed by the reactant. The "barrier" to reaction is not some obscure activation energy, E_a , which must be overcome by raising the temperature of one particular region to a high enough level; rather it is the "resistance" or thermal inertia of the entire system that must be overcome. The thermal inertia is $\int_{T_0}^{T_s} C(T) dT + \Delta H_v$, and the reciprocal of that resistance is the "conductivity" of the reaction wave, which is its rate coefficient, k_t .

PYROLYSIS RATES AND STRUCTURAL MICROSCOPIC REALITIES FOR COAL

Kinetic data for the devolatilization rates of microscopic coal particles of varying diameter, heated in a CO_2 laser beam were reported previously (4, 5). The data at a constant input laser flux of 300 W/cm^2 for particles of 51-, 105-, and 310- μm average diameter are shown in Figure 2. The data show clearly that the time required for complete devolatilization increases monotonically with increasing particle diameter, as would be predicted by the flux-driven model of Figure 1. The effect of varying the incident laser flux for a given particle size was also studied.

For a more careful analysis of the data, it should be noted that the percentage mass loss versus time curves in Figure 2 have characteristic s-shapes. Since final volatility yields, $V(\infty)$, are approached only asymptotically as $t \rightarrow \infty$, it is most realistic to express the rate of the devolatilization reaction in terms of the time required for the particle to devolatilize to half its maximum value. That half life or $t_{1/2}$ -value corresponds to the inflection point of the s-shaped curve. All the data are summarized in Figure 3, where the measured $t_{1/2}$ data points are plotted as a function of the incident laser flux for the three particle sizes studied. For the cubic particle with sides of width a_0 , as depicted in Figure 1,

$$t_{1/2} = \frac{a_0}{2k_t} = \frac{a_0 \rho}{2k_t I_{\text{abs}}} = \frac{k' D_p}{(I - I_q')} \quad (4)$$

where I_q' is an effective loss flux and k' is a constant of proportionality which is linearly proportional to the thermal inertia of the devolatilization reaction, but which is also related to the shape of the particle and its orientation in the beam. The average particle diameter is D_p . The predictions of Equation 4 are also shown in Figure 3 as the dashed lines. The effective loss fluxes, I_q' , were taken as 50 W/cm^2 for the 51- μm particles, 25 W/cm^2 for the 105- μm particles, and 10 W/cm^2 for the 310- μm particles. These losses are mainly associated with conduction-convection to the cold surroundings, and their choice is discussed in detail elsewhere (5, 6). A constant k' -value of 1.46 kJ/cm^3 for all sizes gives the best fit to the data. The reasonable agreement between the data points and the theory curves predicted by Equation 4 tends to confirm the reasonableness of its derivation. It suggests that even on the microscopic level of particles as small as 50 μm , the pyrolysis process proceeds at a rate determined by the heat-transport-limited speed with which the devolatilization wave is driven through the particle by the heat source flux. The pyrolysis "rate constant" is determined by the thermodynamic properties of the medium, and no further assumption regarding a reaction kinetic mechanism appears to be necessary.

In terms of the actual thermal structure of the pyrolysis wave front, the data containing the most detailed spatial resolution were reported by Lee, Singer, and Chaiken (11) for large coal cylinders 1.8 cm in diameter and 5 cm high. Temperatures were measured every 3 mm. Their temperature profiles, obtained with the same laser but at much lower fire-level heat fluxes, are summarized in Figure 4.

They also obtained x-ray density profiles which showed that the reaction zone of active pyrolysis and devolatilization is characterized by a minimum density of 0.2 g/cm^3 . These minimum density points are shown in Figure 4 superimposed on their measured temperature profiles. That reaction zone of minimum density is bounded on the cold side by unreacted coal ($\rho = 1.33 \text{ g/cm}^3$) and on the hot side by a consolidated char residue ($\rho = 0.85 \text{ g/cm}^3$). The reaction zone temperature corresponding to these minimum density points is $440\text{--}475^\circ \text{C}$.

The minimum density zone may be viewed as a "fizz zone" of active devolatilization composed of "frothing" liquid bitumen. The liquid bitumen consists of high-molecular-weight pyrolysis products, and it is frothing because lower molecular weight gases and tar vapors are bubbling through it. The bubbling "fizz zone" is also physically transporting the frothing mass of charifying liquid bitumen into the mass of previously formed char above it. The consolidated char of higher density is thus a compacted residue of the frothing mass of charifying liquid. Some secondary char-forming reactions are also occurring in the char layer above the fizz zone, as pyrolysis vapors diffuse through that cap of higher temperature char.

The data of Lee, Singer, and Chaiken also show clearly that the pyrolysis wave front propagates inward at a velocity that is proportional to the radiant flux; however, as the insulating char layer at the surface thickens in time, the surface temperature increases and flux losses to the cold surroundings increase markedly. It is not surprising, therefore, that the velocity of their pyrolysis wave front diminishes in time. Note also that the reaction zone temperature, however, remains essentially constant at $440\text{--}475^\circ \text{C}$, quite independent of the magnitude of the source flux that drives it, or the resultant velocity of the pyrolysis wave front. At their highest laser flux, the maximum temperature of the char layer at the surface was $760\text{--}800^\circ \text{C}$. Because of the char layer expansion and swelling, the final surface is at a negative displacement relative to the original surface position at 0.0 cm .

That surface temperature may be considered to be the "source temperature" in such experiments since it is the char layer at the surface that directly absorbs the laser flux as time proceeds. Heat is then conducted through that char layer to the reaction zone below. Thus, although the source temperature is as high as $760\text{--}800^\circ \text{C}$ for the higher flux data, the real temperature of the coal mass that is pyrolyzing and devolatilizing is only $440\text{--}475^\circ \text{C}$, and it would be incorrect to assign that char layer temperature to the reacting coal. It should also be noted that if the temperature of the coal sample or "particle" were measured optically from the surface spectral radiance, one would, of course, obtain only the surface temperature of the char residue and not the temperature of the reacting coal.

Structural data will now be presented that reveal the morphological changes in the coal structure that result from the propagation of such a pyrolysis wave front. The microscopic data will be presented for fine coal particles such as those used to obtain the data in Figures 2 and 3, and also for large coal samples comparable in size to those for which the data in Figure 4 were obtained. Scanning electron microscope (SEM) photographs of a coal particle exposed for 100 ms to a laser flux of 100 W/cm^2 are shown in Figure 5. The same particle is shown at two magnifications. The measured weight loss was only about 1 pct, and it can thus be inferred that the exposure time barely exceeded the induction time required for the surface of the particle to reach the decomposition temperature. There is, nevertheless, clear evidence that liquid bitumen was formed near the surface of the particle. That bitumen was oozing out from between the bedding planes while the particle was being heated, but after the beam was turned off, the surface cooled and the bitumen resolidified in the form of ridges. Those ridges are clearly seen to be oriented parallel to the bedding planes. A few blow holes are visible in those ridges of resolidified bitumen, but there are many more unbroken bubbles containing volatiles that were probably never emitted from the heated surface. Most of those volatiles have recondensed as liquid tars that are probably still contained within the bubble enclosures. Clearly, although devolatilization may have occurred within those bubbles, the process was not yet registered as a weight loss since the volatiles never broke through the bubble walls. The SEM photographs in Figure 5 suggest that the extent of thermal pyrolysis in a particle may be more extensive

than that obtained from the devolatilization weight loss. In order to be more precise, one should therefore distinguish between those two sequential processes. Pyrolysis or decomposition occurs first, and volatile emission occurs later. The photographs clearly illustrate the nature of the mass transport limitation involved in the transition between the generation of volatiles by thermochemical pyrolysis and their subsequent emission by bubble transport and rupture. It is only after the latter process is complete that a finite weight loss is registered.

The SEM photograph shown in Figure 6 is a later stage in the same process. It is a particle exposed for a time of 400 ms at a laser flux of about 125 W/cm^2 . Based on its mass loss, the particle is somewhat more than half devolatilized, and it has clearly not reacted uniformly throughout its extent. Only the upper half of the particle (seen in Figure 6 as its right side) has devolatilized. The lower half of the particle (on the left) is essentially unreacted. It is the original coal structure. The laser beam was incident on the upper surface of the particle, and only the upper portion was devolatilized during the exposure time. It devolatilized into a dome or bubble, and after the volatiles contained within that dome were vented through blowholes, the whole structure seems to have started to collapse under its own weight. But, as it was collapsing, the higher molecular weight pyrolysis products that comprise the dome wall were simultaneously solidifying into a char. When they did solidify, a wrinkled skin residue was left.

The devolatilization wave thus appears to have traversed more than half way through the particle by the time the laser beam was turned off. The particle then cooled, and the devolatilization process was quenched with the pyrolysis wave "frozen" in place. Clearly the thickness of the wave front is substantially smaller than the particle diameter, and one can infer a wave front thickness of no more than $50 \mu\text{m}$ from the SEM photograph. Similar examples of such partially devolatilized particles are shown in Figure 7. Those particles are somewhat smaller in diameter and were exposed to a laser flux of about 100 W/cm^2 for about 1 s. Based on their average weight loss, the particles were about two-thirds devolatilized. In all four instances, the particles are viewed from the top, which was the surface on which the laser beam was incident. Blowholes and char residues are seen on the top portions of the particles. Unreacted coal residues with their cleaved edges and ledges are clearly visible at the bottoms of the particles. Again, the pyrolysis waves are frozen in place after having transversed only part of the way into the particles.

Experiments were also conducted with macroscopic coal samples of Pittsburgh seam bituminous coal, and those results are shown in Figure 8. The dimensions of the sample studied in Figure 8 and its orientation during laser exposure are sketched at the top of the figure. The face to be inspected by the SEM was deliberately cleaved some $20\text{-}30^\circ$ beyond the vertical so that it would be "in the shadow" of the upper, irradiated surface. Exposure of the samples to a laser flux of $100\text{-}125 \text{ W/cm}^2$ for 2 s resulted in coking of the surface and its upward expansion as the char layer built up in thickness. Only the edge of the pyrolysis wave front moves down the cleaved face during that exposure time, and it is the edge that is viewed by the SEM, as illustrated in the sketch. The SEM photographs of the transition zone between the coal below and the char above are shown at three magnifications, with the largest magnification on the right. The transition region appears to be quite sharp. Despite the complications associated with the viewing angle, the swelling and frothing of the char layer, and the waviness of the pyrolysis front, one can estimate a reaction zone thickness for the quenched pyrolysis wave that is no larger than about $50 \mu\text{m}$.

One must also realize that there is some thermal inertia in such a wave front so that its progression does not stop instantaneously after the laser source is turned off, especially if the wave front is being driven by the temperature gradient and thermal inertia of a char layer above it. The wave will inevitably progress to some extent during the decay time, and thermal diffusion during that same period may also thicken the wave front. The quenched "dead" wave seen in Figure 8 may therefore be somewhat broader than an active "live" wave. Such thermal inertia effects are even more significant for particles that are heated omnidirectionally in a furnace or a flow reactor than for the unidirectionally-heated particles described here.

A macroscopic sample of a Wyoming coal with a low-free swelling index (Hannah seam) was also studied by the same technique, and those results are reproduced in Figure 9. There was substantial cracking of the sample caused by the mechanical stresses induced by the high temperature gradient laser exposure (100-125 W/cm² for 2 seconds). Those fractures provide a revealing, three-dimensional view of the structure of the transition zone between the char above and the coal below. The position of the pyrolysis wave front is indicated in Figures 9A-F by the arrows at the edges of the SEM photographs. A detailed analysis of the structure is given elsewhere (6), but again the data give an intrinsic width of the wave front that is less than 50 μm.

These SEM photographs in Figures 5, 6, 7, 8, and 9 clearly reveal the existence of the pyrolysis wave front and its structural reality on the microscopic scale. They strongly support the newer viewpoint that the process occurs in the form of the inward progression of a pyrolysis wave front from the exposed surface. Even for small particles, these microscopic realities directly contradict the traditional viewpoint that the reaction process occurs isothermally throughout the particle.

PYROLYSIS AND DEVOLATILIZATION OF PMMA

Long cylinders of polymethylmethacrylate (PMMA) with diameters of 0.45 cm were oriented on end, and exposed to the same CO₂ laser beam. The pyrolyzing upper surface of the rod maintained its circular cross section as the surface regressed downward along the axis of the cylinder. The weight or mass loss per unit area, Δm, was measured as a function of exposure time in a given laser flux. The data are summarized in Figure 10. The good linearity of the Δm versus time curves indicate that steady-state conditions were obtained. Lines are drawn in Figure 10 for the least squares fits to the data points at each flux level. The lines are well represented by the equation

$$\Delta m = \dot{m} (t - \tau). \quad (5)$$

The slope of each line thus represents the steady-state devolatilization rate, \dot{m} , at each flux, and the horizontal intercept is the induction time, τ , at that flux. Clearly, the induction time is simply the time required for the surface of the sample to be heated to the devolatilization temperature. The steady-state rates are plotted in Figure 11 as a function of the net incident flux $I(1 - r) = 0.93 I$, where the reflectance, r , is taken as 7 pct. A least squares fit to the five sets of data points in Figure 11 gives

$$\dot{m} \text{ (mg/cm}^2\text{s)} = 0.72 \text{ (mg/J)} [0.93 I - 9.8] \text{ (W/cm}^2\text{)}. \quad (6)$$

The inferred steady-state loss flux is therefore $I_0 = 9.8 \text{ W/cm}^2$, and the rate coefficient for the pyrolysis and devolatilization of PMMA is therefore $k_t \text{ (PMMA)} = 0.72 \text{ mg/J} = 3.01 \text{ g/kcal}$. Its reciprocal, $1/k_t = 332 \text{ cal/g}$, is the thermal inertia of the pyrolysis wave. According to Equation 3, the thermal inertia is given by $\int_{T_0}^{T_s} C(T)dT + \Delta H_v$. Taking the decomposition temperature for PMMA as 400 °C (12), the heat capacity data reported by Bares and Wunderlich (13) give $\int_{25}^{400} C(T) dT = 196 \text{ cal/g}$. The calorimetrically measured value for the heat of depolymerization of PMMA (corrected to 400 °C) is 126 cal/g (14). The sum, 322 cal/g, is therefore the calculated thermal inertia of the system. The thermodynamically predicted rate constant obtained from Equation 3 for the pyrolysis and devolatilization of PMMA is thus in excellent agreement with the measured value obtained from Figure 11. Furthermore, the measured slope from Figure 11 for data obtained at radiant fluxes of 12-115 W/cm² is in quite good agreement with the slopes measured independently by Vovelle, Akrich, and Delfau (15) and by Kashiwagi and Ohlemiller (12). Their data were obtained at radiant fluxes in a much lower range of 1.4-4.0 W/cm². A detailed analysis of both their data is presented elsewhere (6). Their data were for vertically oriented slabs of PMMA with much larger cross-sectional areas of 10 x 10 cm² and 4 x 4 cm², respectively. Accordingly, their loss fluxes were only about 1.0 and 1.5 W/cm², respectively, but their plotted slopes were essentially the same as those in Figure 11.

The coal data presented earlier can also be used to obtain estimates for the coal's k_t -value. The macroscopic \dot{m} versus I curves reported by Lee, Singer, and Chaiken (11) have also been analyzed in detail elsewhere (6), and their measured slope gives $k_t = 0.75$ g/kcal for coal. The microscopic particle data shown in Figure 3 can also be used to infer a rate coefficient for coal of $k_t = \rho/2k' = 1.91$ g/kcal, which is a factor of 2-3 higher. Clearly those data for coal are substantially less accurate than the PMMA data. A difference of a factor of 2 or 3 for independently-measured rate coefficients for coal is probably the best one can expect considering the complexities associated with the coal's insulating char layer, the uncertainties in the shape factors for the fine particles, the in-depth absorption of the laser beam which is significant for particle dimensions but trivial for large samples, the two orders of magnitude range in incident fluxes, and the three orders of magnitude differences in sample size. Thus there is considerable uncertainty in the k_t -value for coal, but the available data suggest that it is somewhat lower than the value for PMMA. Clearly, except for the complication of the coal's char layer residue and its more complex devolatilization thermodynamics, there appear to be no other extraordinary differences in the pyrolysis and devolatilization behavior for the two substances. Both pyrolysis rates are describable in terms of the progression of a decomposition wave whose speed of propagation is controlled by thermodynamic transport constraints.

Returning to the PMMA data, Kashiwagi and Ohlemiller (12) and Kashiwagi (16), also measured surface temperatures during devolatilization, and those data are shown in Figure 12. Their data, obtained at two flux levels show that \dot{m} -values are insignificant until some threshold temperature is approached, at which point the rate becomes exceedingly rapid as the \dot{m} versus T curve turns vertically upward. Above the threshold temperature, the rate of pyrolysis and devolatilization becomes virtually insensitive to the surface temperature. For the exposed surface to reach the decomposition temperature of 350-400° C, a minimum threshold heating flux is required in order to overcome the loss flux, I_L . A theory curve is shown in Figure 12 which is a simple step function at T_S , and it represents the assumption implicit in the derivation of Equations 2 and 3.

According to the assumption used for the new model, there is no devolatilization in the horizontal portion of the curve ($\dot{m} = 0$) until the surface temperature of the sample reaches the decomposition temperature, T_S . Once the surface reaches the decomposition temperature T_S , the rate becomes finite and one is in the vertical portion of the step function. The rate is then controlled entirely by the source flux intensity, and the temperature of the reacting surface becomes both invariant and virtually irrelevant.

The model represented by Equations 2 and 3 thus uses a step function to approximate the finite curvature of the transition depicted in Figure 12. In the horizontal portion of the step, the surface is heating up in the input flux, but there is no devolatilization occurring because the temperature is too low. Once the temperature reaches T_S and significant pyrolysis and devolatilization begin, one transits into the vertical portion of the step, and the system is under heat transport control.

It is also interesting to compare the measured induction times for the onset of the pyrolysis and devolatilization process for the PMMA samples with those predicted on the basis of the measured T_S value of 400° C and the exact solution to the time-dependent heat transport equation. For a semi-infinite solid whose surface is heated by a constant source flux, Carslaw and Jaeger (17) give:

$$\tau = \frac{\pi}{4} C \rho \lambda (T_S - T_0)^2 / [I(1-r) - I_L]^2. \quad (7)$$

The time required for the surface to reach the temperature T_S is the induction time, τ . The system is initially isothermal at $T_0 = 25^\circ$ C. The heat capacity, C , is taken as the average value for the temperature range between T_0 and T_S , which is 0.52 cal/g °C (13). The density ρ is 1.18 g/cm³, and the thermal conductivity λ is taken as 4.5×10^{-4} cal/cm s °C (14). The source flux is taken as $I_{\text{abs}} = I(1-r) - I_L$.

The comparison between the measured τ -values from Figure 10 and those calculated from Equation 7 is shown in Table 1. The comparison is made for two cases: one with the measured steady state loss flux of $I_L = 9.8 \text{ W/cm}^2$; the other for $I_L = 0$. Initially at $t = 0$, the entire sample is at ambient temperature and $I_L = 0$; however, as $t \rightarrow \tau$, $I_L \rightarrow 9.8 \text{ W/cm}^2$. Clearly during the non-steady-state induction period as the surface temperature increases from $T_0 = 25^\circ \text{ C}$ to $T_3 = 400^\circ \text{ C}$, the loss flux, which is due mainly to conduction and convection to the cold surroundings, increases from 0 to 9.8 W/cm^2 . The loss flux is clearly time-dependent, but its average value should vary between those two limiting cases. The table clearly shows that the measured τ -values fall between the two predicted limiting cases. The only exception is the measured τ -value at the highest flux which is about a factor of two higher than the calculated value. That difference is attributed to the finite absorption depth of the laser beam. At low fluxes that absorption depth is trivial compared to the characteristic width of the subsurface temperature profile; however, at the highest flux, the two may be of comparable dimensions. Such in-depth absorption is significant at the the highest flux, and a larger mass near the surface is actually heated by the flux than is calculated from the simple theory from which Equation 7 was derived. As a result, the actual induction time required for the surface to reach T_3 for in-depth absorption is longer than that calculated on the assumption that the flux is deposited entirely at the surface.

Table 1. - Comparison of Measured Induction Times for the Laser Pyrolysis of PMMA with Theoretical Calculations of Equation 7

Laser Flux, W/cm^2		Induction Time, τ , s		
Incident I	Net $I_{\text{abs}} = I(1-r) - I_L$	Measured	Calculated, Equation 7	
			$I_L = 9.8 \text{ W/cm}^2$	$I_L = 0$
115.0	97.2	0.101	0.057	0.047
71.0	56.2	0.160	0.169	0.123
42.5	29.7	0.50	0.605	0.342
23.2	11.8	1.83	3.84	1.16
12.4	1.73	6.70	178	4.04

It should also be noted that the theory curves in Figure 3 for coal particles are based on the steady state condition and are uncorrected for such induction time delays. At the higher fluxes, especially for the larger particles, the τ -corrections are small in comparison to the steady-state $t_{1/2}$ -values. The τ -corrections are however significant at the lower fluxes for the smaller particles. Nevertheless, there is also a decay time correction required, as discussed earlier. The pyrolysis wave's thermal inertia results in some continuing propagation even after the source flux is turned off. These non-steady-state corrections for induction time and decay time would tend to counteract one another.

PYROLYSIS AND DEVOLATILIZATION IN DUST FLAME PROPAGATION

The flame propagation processes in pulverized coal-fired burners or in accidental dust explosions (18) are examples of combustion processes in which the pyrolysis and devolatilization of the solid fuel particles play a key role. Flame propagation in dust-air mixtures involves three sequential processes (19): heating and devolatilization of the dispersed dust particles; mixing of the emitted volatiles with air in the space between particles; and gas phase combustion of the premixed fuel-air mixture. Each sequential process has its characteristic time constant: τ_{dv} , τ_{mx} , and τ_{pm} . The resultant burning velocity of the dust-air flame, S_u , will be given by $S_u = (\alpha/\tau_e)^{1/2}$ where α is the effective diffusivity for heat and/or free radical mass transfer across the flame front, and τ_e is the effective time constant for the completion of the above sequence of processes. The slowest of those processes will be the rate-limiting process, and accordingly, the resultant τ_e will be controlled by the slowest of those τ -values.

For very fine dust particles at low, lean-limit concentrations, the first two processes are so rapid that the propagation rate is controlled by the last process:

gas-phase combustion. Since that is essentially the same process that controls homogeneous, premixed, gaseous flames, dust flame behavior in those limits is virtually identical to that of an equivalent homogeneous gas-air mixture of the dust's volatiles (20, 21). Thus for very fine dust particles at lean-limit concentrations, each particle is completely devolatilized within the flame front, and the lean limit concentration of the dust-air mixture is determined by the total combustible volatile content of the dust. For example, the lean-limit mass concentration for fine polyethylene, $\text{CH}_2-(\text{CH}_2)_n-\text{CH}_3$, a dust that devolatilizes completely in its lean-limit flame, is identical to that of homogeneous gas-air mixtures of the saturated alkanes (20, 21).

For homogeneous gas flames, there exists a minimum burning velocity for natural convective quenching of about 3 cm/s, below which normal flame propagation is impossible (22, 23). For dust flames, the limit burning velocity appears to be somewhat higher for a variety of reasons (24). For a homogeneous gas flame of burning velocity S_u , the characteristic width of the flame front is $\delta = \alpha/S_u$ and the characteristic time for the completion of the homogeneous gas phase reactions is $\tau_{pm} = \delta/S_u = \alpha/S_u^2$. Setting $\alpha = 0.55 \text{ cm}^2/\text{s}$ and $S_u = 3 \text{ cm/s}$ for the limit burning velocity gives $\tau_{pm} = 60 \text{ ms}$. That 60 ms is the characteristic time required for the completion of the gas-phase reactions, and if the rate processes are slower than that, the normal high-temperature flame propagation process is quenched by natural convection (23). For heterogeneous dust-air flames the situation appears to be somewhat more complicated. The limit velocities appear to be about a factor of 2 higher, but at the same time the flame zone thicknesses appear to be broader (24). A higher S_u would, for homogeneous flames, normally be associated with thinner flame fronts according to the previous equation, $\delta = \alpha/S_u$. A higher burning velocity and a thicker flame front for dusts suggest that the dust flame is always somewhat accelerated by turbulent vortices which enhance the diffusivity factor, α , increasing it to a value that is higher than the normal laminar one (24). Those vortices are associated with the dust fuel concentration, which is intrinsically inhomogeneous on the scale of either the particle diameter or the distance between particles. In any case, that complication for dust flames leaves one with an uncertainty in the proper choice for τ_e for the heterogeneous flame. It will be here assumed that for heterogeneous flames, the higher S_u at the limit and the wider flame zone thickness (24) give a τ_e that is about a factor of 2 longer than for homogeneous flames, so that 120 ms is chosen for τ_e . That value is thus the maximum time available for pyrolysis and devolatilization. If the process takes any longer, the volatiles are emitted in the burned gases, which is too late for them to contribute to the propagation process within the flame front.

As dust concentrations increase above their lean limit values, or as the dust particles become coarser, the heating and devolatilization process will begin to become rate limiting. In the former case, as stoichiometric concentrations (with respect to the volatiles) are approached, S_u for hydrocarbon-like dusts approaches its maximum value of about 40 cm/s (25). Since τ_e varies as $(S_u)^{-2}$, that order of magnitude increase in S_u reduces τ_e by two orders of magnitude: from 120 ms to only about 1 ms. For such rapidly propagating dust flames, only the surface regions of the dust particles can contribute volatiles to the flame. The flame "rides the crest" of a near-stoichiometric concentration of volatiles regardless of the initial dust loading. That devolatilization rate limitation is responsible for the absence of a "normal" rich limit of flammability for dusts. Although excess fuel volatiles may continue to be emitted in the burned gases at high dust loadings, they are emitted too late to dilute the flame front with excess fuel vapor (18, 20, 21).

Data for the particle size dependence of the lean limits of flammability for coal and PMMA, as measured in a 20-L chamber (26), are shown in Figure 13. They show clearly how the pyrolysis and devolatilization rate process becomes rate limiting as the dust particles become coarser. The curves for coal and PMMA have similar shapes. The initially flat region demonstrates a lean limit that is independent of particle size as long as the particle diameter is small enough. The smaller particles can all totally devolatilize in the time available, and the system behaves as an equivalent homogeneous premixed gas. As diameters increase, the

curves turn upward at some characteristic diameter because of the devolatilization rate limitation, and a size dependence begins to appear. As shown earlier in Figures 2 and 3, for a given heating flux the devolatilization time increases linearly with particle diameter. Thus the pyrolysis and devolatilization rate limitation appears to adequately explain the shapes of the curves. For a fixed flame flux, the time required for devolatilization τ_{dv} will vary linearly with the particle diameter D_p . Below some characteristic diameter, $\tau_{dv} \ll \tau_{pm}$, the particles can devolatilize completely in the time available, and τ_p is controlled by the gas phase combustion reactions. In that range of fine particle sizes there is no size dependence. However, as $\tau_{dv} \rightarrow \tau_{pm}$, the devolatilization rate process becomes significant in the overall flame propagation process and a particle size dependence begins to appear. For still coarser sizes, $\tau_{dv} \gg \tau_{pm}$, and the rate of devolatilization becomes rate controlling. Only the surface regions of the coarser dust particles can then devolatilize in the 120 ms that is available for flame propagation, and hence, a higher dust loading is required to generate a lean limit concentration of combustible volatiles. The curves must therefore turn upward. Eventually, when the particles are so coarse that an excessive dust loading is required, then other thermal quenching processes become significant, and the critical diameter is reached above which propagation is impossible even at the highest dust concentrations. Those critical diameters are the vertical asymptotes of the curves in Figure 13.

A more quantitative analysis is possible using the pyrolysis and devolatilization rate constants reported here for coal and PMMA. The coal value was uncertain by a large factor, but it was nevertheless lower than the k_t -value for PMMA, which was 3.01 g/kcal. According to Equation 3, when exposed for a time t to a net flux I_{abs} , a devolatilization wave front will travel a distance $x = \dot{x}_0 t = k_t I_{abs} t / \rho$. For dust flames at their limits of flammability, the I_{abs} and t values are comparable for the two dusts. For PMMA, the rate constant is higher than for coal, and its density is only slightly lower. Thus, Equation 3 predicts that the characteristic diameter for PMMA should be somewhat larger than the value for coal. The data curves in Figure 13 support that expectation.

A prediction of the absolute magnitude of the characteristic diameter is also possible. As indicated earlier, the time available for devolatilization within a heterogeneous flame front propagating at the limit velocity is $t = 120$ ms. But what value is one to use for I_{abs} when the particle is being heated in a flame front? The major uncertainty in predicting the characteristic diameter is the uncertainty in estimating, I_{abs} , the effective or net heating flux to which the particles are exposed as they approach, enter, and traverse through the flame front. For homogeneous gas flames, radiation from the burned gases to the unburned fuel is usually not significant because the unburned gaseous mixture has a trivial absorptivity. That is not the case for dust particles, so that well before the particles actually enter the flame front, they will absorb the radiance emitted from the hot combustion products, which consist of burned gases, soot, and char. Typically, hydrocarbon flames exhibit a fairly constant limit flame temperature of 1400 to 1500 K, and the Planck radiance at those temperatures is 5-7 cal/cm²s. But for a spherical particle approaching a flame front, that radiance is seen only by its forward-facing hemisphere. That radiance will however be seen for a considerably longer time period than the particle's 120-ms residence time in the flame front. As the particle heats up in that radiance, it will, however, lose an increasing fraction of that radiance by conduction and convection to the surrounding cold air. It is difficult to estimate the effects of that radiant heat transport process, but it is clear from the previous estimate of the particle loss fluxes, which were as high as 50 W/cm² for 50- μ m particles at $T_g = 450$ -600° C, that the particle temperatures will remain well below the decomposition temperature during that approach period. The particle could nevertheless be preheated significantly above ambient temperature as it enters the flame front. Upon entering the flame front, there is an additional conductive-convective heat flux from the hot gases within the flame front. That heating flux increases in magnitude as the particle penetrates into the burned gases. As it begins to devolatilize in that

conductive-convective flux, the heat transport process becomes exceedingly complex, and the "blowing effect" of the emitted volatiles markedly reduces the Nusselt number. Realistic estimates are difficult to make; however, in (25) it is estimated that the average power density across a homogeneous, laminar, flame-front is given by $S_u C \rho (T_b - T_u)$. For the dust flames under limit conditions $S_u = 6 \text{ cm/s}$, $C = 0.35 \text{ cal/g K}$, $\rho = 1.5 \times 10^{-3} \text{ g/cm}^3$, and $T_b - T_u = 1500 - 300 = 1200 \text{ K}$. The resultant is an average conductive-convective flux of about $4 \text{ cal/cm}^2\text{s}$. If one adds to that flux about half of the previously estimated radiant flux (since only the forward hemisphere of the particle sees the flame), one obtains $I_{abs} = 7 \text{ cal/cm}^2\text{s}$. For PMMA, the travel distance of the devolatilization wave into the particle during its exposure within the flame front thus becomes $x = k_t I_{abs} \tau_e / \rho = 21 \text{ }\mu\text{m}$. Thus for PMMA the depth of penetration of the devolatilization wave front in the time available for flame front passage under near limit-conditions is about $21 \text{ }\mu\text{m}$. For a square particle heated from two opposing faces, the predicted characteristic diameter would therefore be $42 \text{ }\mu\text{m}$. For a spherical particle in an omnidirectional source flux, the devolatilization of an outer shell $21\text{-}\mu\text{m}$ in depth would actually represent the devolatilization of some 90 pct of the mass of a $75\text{-}\mu\text{m}$ -diameter particle. One should also realize that such omnidirectional heating generates a converging wave front which will accelerate as heat accumulates within the particle. Equation 3 was derived for a planar, steady-state wave front. The converging wave will penetrate farther into the particle during the same exposure time. Accordingly, one estimates that the measured rate coefficient for PMMA should correspond to a characteristic diameter of about $80\text{-}100 \text{ }\mu\text{m}$ for spherical particles. That estimate is also in fair agreement with the data in Figure 13.

CONCLUSIONS

On the basis of a detailed analysis and evaluation of a diverse set of experimental observations reported by many independent investigators, and on the basis of the data reported here for pyrolysis rates and microscopic structure, it is concluded that there is no substantive evidence to support the traditional viewpoint that the coal particle pyrolysis process proceeds isothermally, under chemical rate control, or that it is describable by a unimolecular, Arrhenius function of the source temperature, T_h , to which the coal particles are exposed. The overwhelming weight of evidence shows that the process occurs in the form of a non-isothermal decomposition wave whose propagation velocity is linearly proportional to the net absorbed heat flux intensity and inversely proportional to the overall enthalpy change for the reaction.

The pyrolysis and devolatilization "rate coefficient" is the reciprocal of that overall enthalpy requirement for heating and devolatilization. Although the rate coefficient for Pittsburgh seam bituminous coal is smaller than that for the simple polymer, PMMA, the pyrolysis and devolatilization behavior of the coal is not markedly different from that of PMMA, except for the complications associated with the coal's char layer residue.

At fire and burner level heat fluxes of $10\text{-}100 \text{ W/cm}^2$ and above, the pyrolysis and devolatilization behavior of coals and polymers is realistically describable by the thermodynamic transport-controlled model in which the intrinsic rate of decomposition is described as a simple step-function at the decomposition temperature, T_s . Below T_s the intrinsic rate is near zero. At T_s , the intrinsic rate is so rapid that the system is heat transport controlled. There is no substantive evidence that the temperature of the reactant during pyrolysis and devolatilization can significantly exceed T_s , regardless of the source temperature, T_h , to which it is exposed. For PMMA, T_s is $350\text{-}400 \text{ }^\circ\text{C}$; for the coal it is $450\text{-}600 \text{ }^\circ\text{C}$.

REFERENCES

1. Van Krevelen, D.W. *Coal Typology-Chemistry-Physics-Constitution*, Elsevier, 1961, 514 pp.
2. Badsiock S. and P. G. W. Hawksley. *Industrial Engineering Chemistry, Process Des. Develop.* 9 (1970), p. 521
3. Anthony, D. B. and J. B. Howard. *AIChE Journal*, 22 (1976), p 625.
4. Ng, D. L., M. Hertzberg, and J. C. Edwards. A Microscopic and Kinetic Study of Coal Particle Devolatilization in a Laser Beam. Poster Session Paper No. 83, 20th Combustion Symposium, 1984.
5. Hertzberg, M. and D. L. Ng. NATO Advanced Research Workshop on Fundamentals of Physical Chemistry of Coal Combustion, ed. by J. Lahaye, NATO Series Catalogue, Martinus Nijhoff, to be published 1987.
6. Hertzberg, M., I. A. Zlochower, and J. C. Edwards. Coal Particle Pyrolysis Mechanisms and Temperatures. Bureau of Mines Report of Investigation, to be published 1987.
7. Zielinski, E. *Fuel* 46 (1967), p 329.
8. Freihaut, J. D. and F. J. Vastola. Eastern Section - Combustion Institute, Fall Technical Mtg., Miami Beach, Florida, Nov. 29-Dec. 1, 1978, p 32-1.
9. Solomon, P. R., R. M. Corangelo, P. E. Best, J. R. Markham, and D. G. Hamblen. The Spectral Emittance of Pulverized Coals and Char. 21st Symposium (Int.) on Combustion, to be published 1987.
10. Solomon, P. R., and M. A. Serio. Evaluation of Coal Pyrolysis Kinetics. NATO Advanced Research Workshop on Fundamentals of Physical Chemistry of Coal Combustion, ed. by J. Lahaye, NATO Series Catalogue, Martinus Nijhoff, to be published 1987.
11. Lee, C. K., J. M. Singer, and R. Chaiken. *Comb. Sci. and Techn.*, 16 (1977), p 205.
12. Kashiwagi, T. and T. J. Ohlemiller. 19th Symposium (Int.) on Combustion, Combustion Institute, 1982, p 815.
13. Bares, V. and B. Wunderlich. *J. Polymer Sci., Polymer Phys Edition*, 11 (1973), p 861.
14. Brandrup, J. and E. H. Immergut. *Polymer Handbook*, 2nd ed, J. Wiley and Sons (1975), pp II-425 and V-56.
15. Vovelle, C. R. Akrich, and J. L. Delfau. *Comb. Sci. and Techn.*, 36 (1984), p 1.
16. Kashiwagi, T. *Combustion and Flame*, 34 (1979), p 231.
17. Carslaw, H. S. and J. C. Jaeger. *Conduction of Heat in Solids*, 2nd ed., Oxford, p 75.
18. Hertzberg, M. and K. L. Cashdollar. Introduction to Dust Explosions, in STP 958, *Industrial Dust Explosions*, American Society for Testing and Materials, Philadelphia, PA 1987, to be published.
19. Hertzberg, M., K. L. Cashdollar, D. L. Ng, and R. S. Conti. 19th Symposium (Int.) on Combustion, Combustion Institute, 1982, p 1169.
20. Hertzberg, M., K. L. Cashdollar, and I. A. Zlochower. Flammability Limit Measurements for Dusts and Gases: Ignition Energy Requirements and Pressure Dependencies, 21st Symposium (Int.) on Combustion, Combustion Institute, to be published 1987.
21. Hertzberg, M., I. A. Zlochower, and K. L. Cashdollar. Volatility Model for Coal Dust Flame Propagation and Extinguishment, 21st Symposium (Int.) on Combustion, Combustion Institute, to be published, 1987.
22. Hertzberg, M. Bureau of Mines RI 8127, (1976).
23. Hertzberg, M. 20th Symposium (Int.) on Combustion, Combustion Institute (1984), p 1967.
24. Klemens R. and P. Wolanski. Flame Structure in Dust and Hybrid Mixtures Near the Lean Flammability Limit. Poster Session Paper No. 100, 20th Combustion Symposium, 1984.
25. Hertzberg, M. Bureau of Mines RI 8469, (1980).
26. Cashdollar, K. L. and M. Hertzberg, *Rev. Sci Instrum.*, 56 (1985) p. 596.

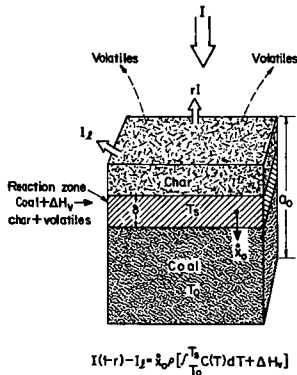


Figure 1. - A schematic idealization of the propagation of a planar steady-state pyrolysis and devolatilization wave front in coal as it is being driven by a plane-wave radiant source flux of intensity, I .

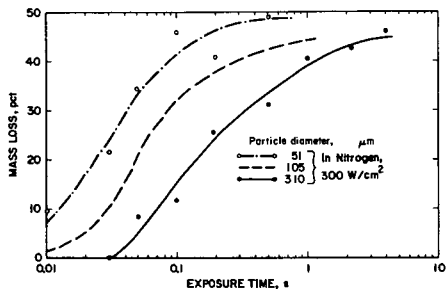


Figure 2. - The devolatilization mass loss for coal particles of 51, 105, and 310 μm diameter as a function of exposure time at a constant laser source intensity of 300 W/cm^2 , from reference 5.

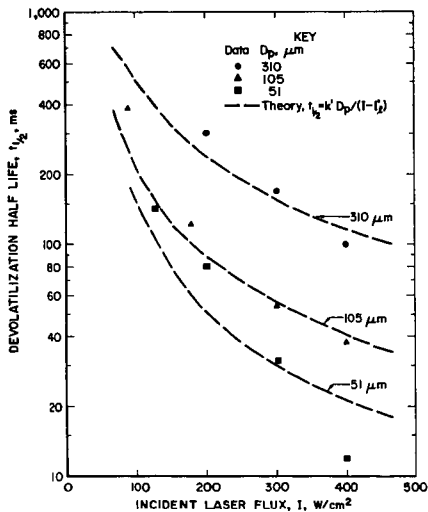


Figure 3. - Summary of the measured half lives for coal particles as a function of laser source intensity for the three coal particle sizes from reference 5. The data points are compared with the theory based on heat transport limitations according to the First Law of Thermodynamics.

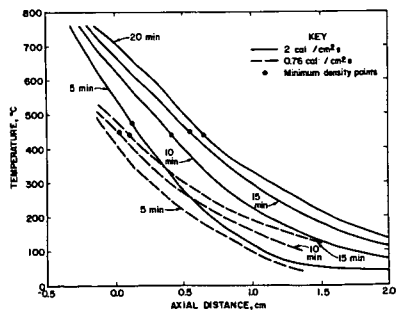


Figure 4. - Measured temperature profiles for coal during pyrolysis and devolatilization as a function of time for two laser intensities, as measured by Lee, Singer, and Chaiken(11).

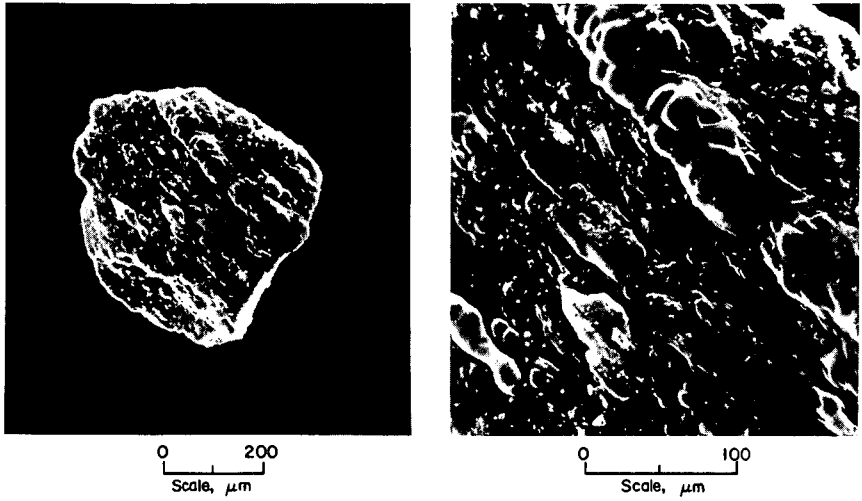


Figure 5. - Scanning Electron Microscope (SEM) photographs of the exposed surface of a coal particle exposed for 100 ms to a laser flux of about 100 W/cm^2 , seen at two magnifications.

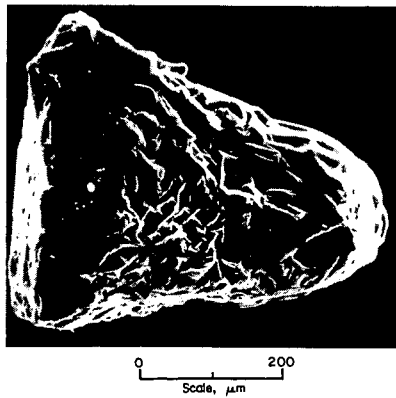


Figure 6. - SEM photograph of a coal particle, which is about two-thirds devolatilized after exposure for 400 ms to a laser flux of about 125 W/cm^2 .



0 50
Scale, μm

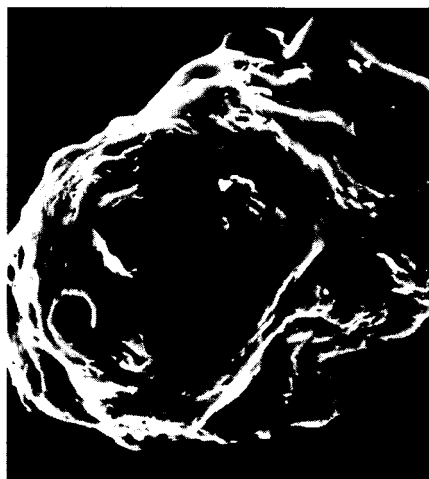


Figure 7. - SEM photographs of four different particles exposed to a laser flux of about 100 W/cm^2 for 1 s. The particles are all about two-thirds devolatilized by the laser flux incident from above.

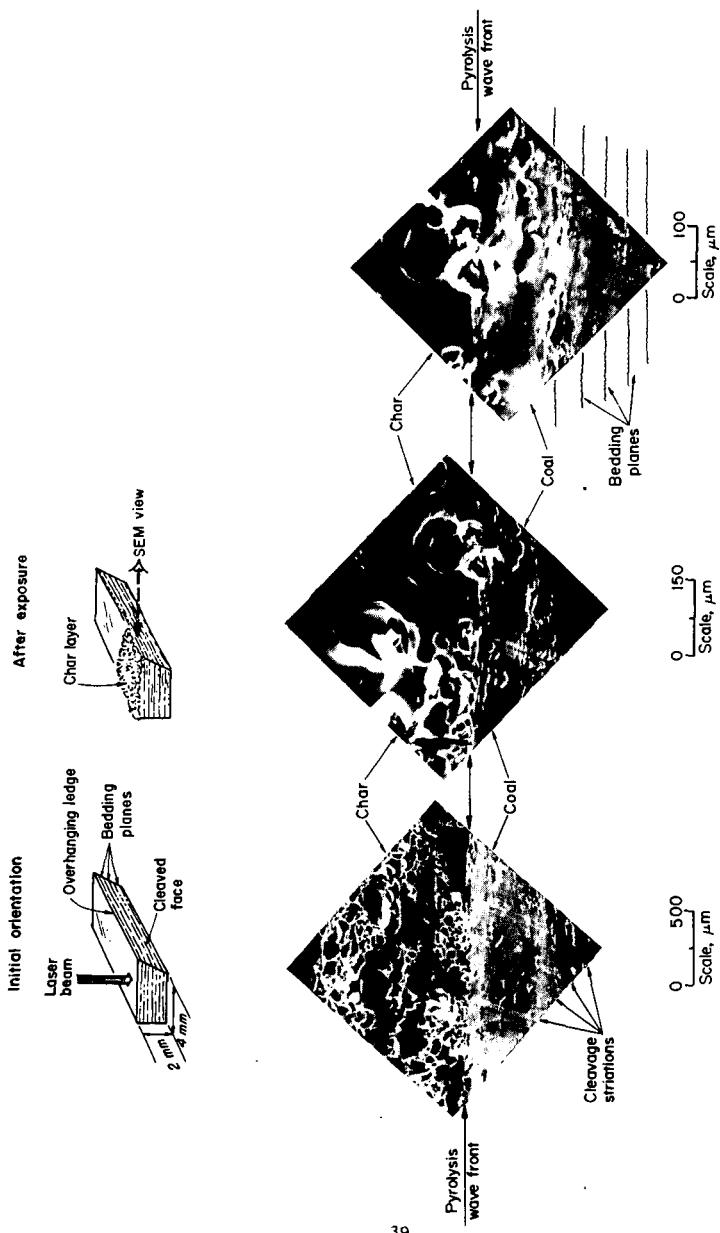


Figure 8. - SEM photographs viewed from the side of a shadowed, cleaved face of a macroscopic sample of Pittsburgh seam bituminous coal exposed for 2 s to a laser flux of 100-125 W/cm². The pyrolysis and devolatilization wave front is viewed at three magnifications.

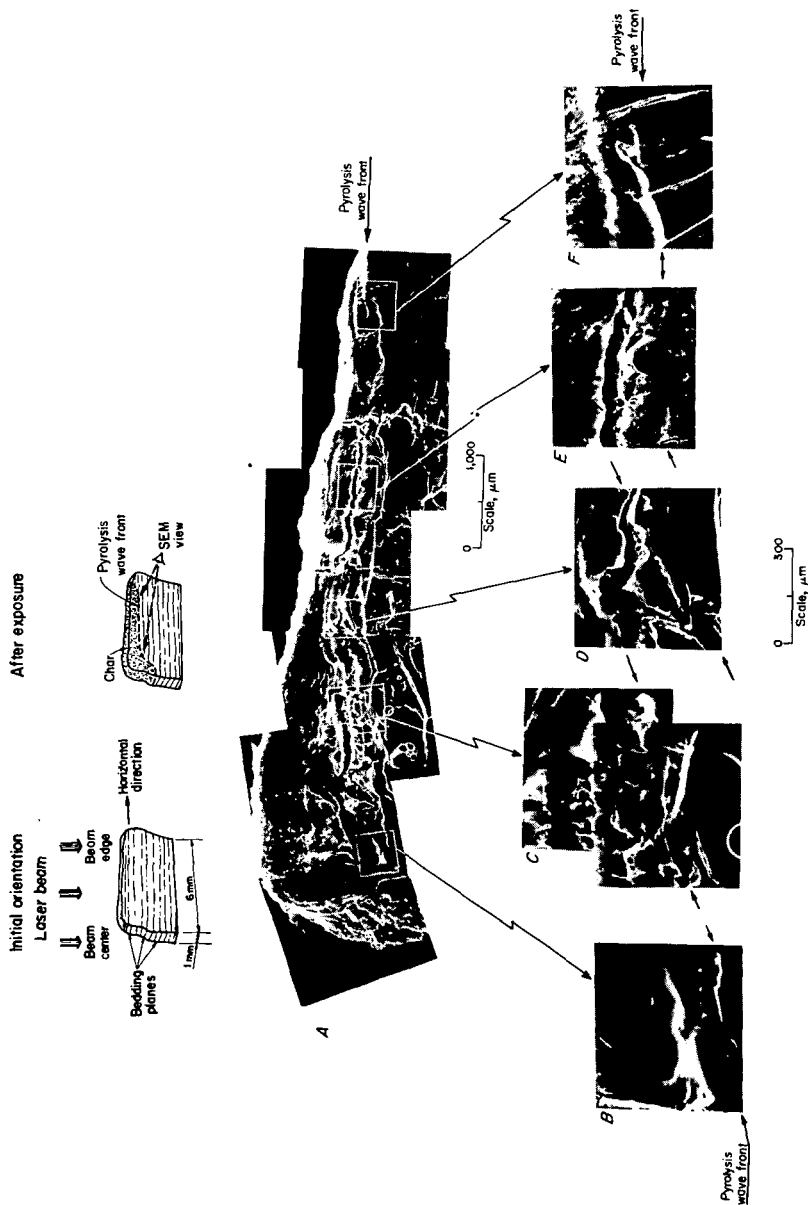


Figure 9. - SEM photographs of a macroscopic sample of the Hannah-seam coal exposed to a maximum laser flux of 100-125 W/cm² for 2 s, as viewed from the side. Lower magnification montage in A; higher magnification views of the pyrolysis and devolatilization wave front in B, C, D, E, and F.

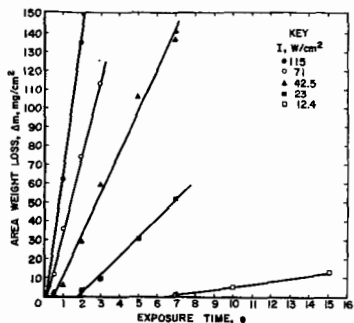


Figure 10. - The measured pyrolysis and devolatilization weight (or mass) losses for 0.45 cm diameter, PMMA cylinders as a function of exposure time for different input laser flux intensities in the range 12 to 115 W/cm².

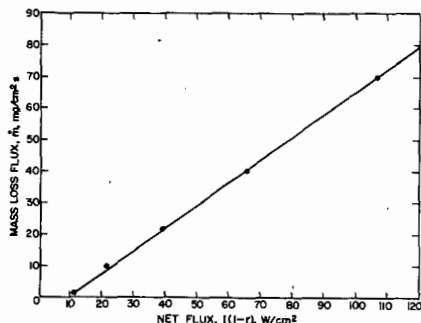


Figure 11. - The measured, steady-state rates of pyrolysis and devolatilization for 0.45 cm diameter PMMA cylinders, as a function of input laser flux corrected for surface reflectance, r .

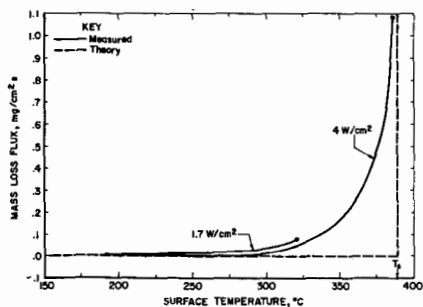


Figure 12. - The measured surface temperatures at various mass loss rates during the pyrolysis and devolatilization of PMMA at two radiant fluxes as reported by Kashiwagi and Ohlemiller. Measured values compared with simplified, step-function theory using a discrete, decomposition temperature, T_s .

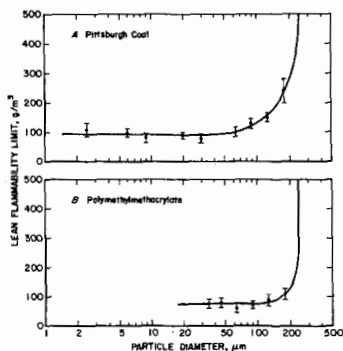


Figure 13. - Lean flammability limit as a function of particle diameter for Pittsburgh seam bituminous coal and polymethylmethacrylate.